Q-dependent electronic excitations in osmium: Pressure- and temperature-induced effects

Yu. S Ponosov*
Institute of Metal Physics, UD, RAS, 620041, S. Kovalevskaya str. 18, Ekaterinburg, Russia

V. V. Struzhkin and A. F. Goncharov
Geophysical Laboratory, Carnegie Institution of Washington, 5251 Broad Branch Road NW, Washington, DC 20015, USA

S. V. Streltsov
Institute of Metal Physics, UD, RAS, 620041, S. Kovalevskaya str. 18, Ekaterinburg, Russia
and Ural State Technical University, Mira St. 19, 620002 Ekaterinburg, Russia
(Received 15 July 2008; revised manuscript received 6 November 2008; published 5 December 2008)

Raman scattering by electrons and phonons has been studied in single crystals of the 5*d* transition-metal osmium under pressures up to 60 GPa in the temperature range of 10–300 K. An anomalous increase in the electronic light-scattering cross section was found in the pressure range of 20–30 GPa with the use of green and blue excitation wavelengths. At these conditions, we observe an appearance of well-defined electronic peaks at ~580 cm^{-1} for the wave-vector direction $\mathbf{q}\|[0001]$ and at ~350 cm^{-1} for $\mathbf{q}\|[10\bar{1}0]$. The comparison of **q** dependencies measured and calculated from the first-principles spectra suggests a strong volume- and temperature-dependent renormalization of the energies and damping of the electronic states near the Fermi level.

DOI: 10.1103/PhysRevB.78.245106 PACS number(s): 62.50.−p, 78.30.Er, 71.18.+y, 72.10.Di

I. INTRODUCTION

During the past decades inelastic electronic light scattering (ELS) has been widely used for studies of the superconducting gap in ordinary metals and high-temperature superconductors (HTSCs). The gap excitations have been studied in pure Nb, A15 compounds, and layered metals[1–4] but the electronic scattering in the normal state has not been identified. In contrast, an intense, broad, and almost structureless Raman response has been observed in the normal state of HTSCs.[5–8] Strongly temperature-dependent electronic Raman spectra have been reported for a number of correlated systems.[9,10] Usually these observations have been discussed within a $\mathbf{q}=0$ assumption based on the smallness of the wave vector $\mathbf{q}\sim 1/\delta$ (δ is the penetration depth, which is usually of the order of 10–100 nm for visible wavelengths) and in the case of A-15 and HTSCs also due to the smallness of the ratio ζ/δ (ζ is the coherence length). Since the probed momentum space is very limited (**q** is small) and because of the screening of the charge fluctuations, the ELS cross section is very small in metals. In order to explain a large cross section for ELS in HTSCs and correlated systems, different mechanisms have been proposed to extend the momentum volume: marginal Fermi liquid,[11] impurity relaxation,[12] nested Fermi liquid,[13] inelastic scattering,[14–17] and electronic correlations.[18] All these approaches suggest a strong and sometimes frequency-dependent damping of the electronic states $\Gamma(\omega)$ in order to explain the smearing of electronic spectra over a wide frequency range.

In a clean metal with an anisotropic Fermi-surface (FS) intraband electronic scattering may also be observed in the wide frequency range $\omega<v_F/\delta$ (v_F is the electron Fermi velocity) under an assumption of $\omega>\Gamma$.[19,20] In the region of the maximum scattering intensity at $\omega\sim v_F/\delta$ the scattering cross section is determined by contributions from all the electrons at the FS. Thus, the study of the ELS spectra may give independent information about the FS topology. A renormalization of the electron self-energies by any relaxation process such as an electron-phonon (e-ph) and/or electron-electron (e-e) scattering will change the frequency dependence of the Raman response, and therefore, may be studied by performing a detailed analysis of the **q** dependencies of the measured spectra.

The first observation of the momentum dependence of the ELS in the normal state has been reported in the hcp transition-metal osmium.[21] The momentum **q** was tuned by changing the incident laser energy allowing the dispersion of the phonon and electronic excitations to be studied. An abrupt and anisotropic optical phonon frequency softening (2%–3%) was found in the range of $\mathbf{q}\sim 10^6$ cm^{-1} at low temperatures. This anomalous phonon dispersion and broadening, and also the asymmetry of the phonon lines, have been observed in the momenta range corresponding to a crossing of the electron and phonon excitation energies. This is indicative of a strong e-ph interaction. A sharp decrease in the phonon damping has been found at the smallest momenta investigated. This finding suggests the occurrence of the Landau damping threshold.[22] Additionally, the observed **q** dependencies of the self-energies of the optical phonons and electronic excitations in osmium are in qualitative agreement with the theoretical predictions,[22,23] confirming the existence of nonadiabatic effects in the e-ph interaction in transition metals.

The application of pressure may modify both the electronic band structure near the Fermi level and internal scattering processes, which would affect the Raman spectra. This provides an additional tool to study the electronic excitations responsible for anomalous dispersion effects. Experiments at pressures up to 15 GPa have shown that the volume changes contribute no more than 20%–30% to the temperature-

induced hardening of the phonon frequencies in osmium and rhenium,[24,25] confirming the dominant role of the e-ph interaction.[26–28] An anomalous phonon hardening in osmium has been found at pressures higher than 15 GPa under nonhydrostatic conditions.[25] Recently, an anomaly in the c/a ratio of osmium has been observed at pressures of 20–25 GPa (Ref. 29) which was attributed to a possible change in the FS topology.

The goal of this work is to study the changes in fine details of the electronic structure near the Fermi level in the pressure range where the above-mentioned phonon and lattice anomalies have been found. Here we present the experimental observation of ELS in osmium at pressures up to 60 GPa in the temperature range of 10–300 K for different **q** values and directions. First-principles calculations of the frequency dependencies of the electronic scattering cross section have also been performed for comparison with the measured Raman spectra.

II. EXPERIMENT

Platelets of osmium single crystals with (0001) and $(10\bar{1}0)$ orientations which are thinned to 5–10 μm by mechanical and electrochemical polishing were loaded into a diamond-anvil cell and placed in an optical cryostat. The high purity of the crystals ("clean limit regime") was confirmed by the high-resistivity ratio $\rho_{300\ \mathrm{K}}/\rho_{4.2\ \mathrm{K}} > 1000$. Argon was used as the pressure-transmitting medium. The pressure was changed at room temperature to provide quasihydrostatic conditions at low temperatures and was measured using the ruby luminescence method[30] with a temperature correction from Ref. 31. Four laser lines λ_i (740, 633, 514, and 488 nm) of Ar ion, He-Ne, and Ti:sapphire lasers with powers up to 150 mW were used for the Raman spectra excitation. Spectra were collected in a quasibackscattering geometry (~145°) (Ref. 32) with a laser spot of about 20 μm in diameter. The spectra were analyzed using a HR-460 single-grating spectrograph equipped with notch filters and charge coupled device (CCD). The variation of osmium refraction index, n, and extinction coefficient, k, with wavelength allows the wave vector **q** to be tuned in the range $(0.5–1.2)\times 10^6$ cm^{-1} with n being always larger than k,[33] which is favorable for electronic light-scattering observation. The features in the spectra correspond to the Raman tensor components (XX), (YY), and (XY) in the basal plane, where X is parallel to the $[10\bar{1}0]$ direction and Y to the $[11\bar{2}0]$ direction. For the phonon scattering, this is determined by Raman selection rules for an hcp structure (D^4_{6h} space group). The polarization measurements at ambient pressure confirm the validity of such classification for the ELS in the case of scattering from the planes containing the crystal axis.[21] Part of the background signal was produced by the anvil luminescence. To subtract such contributions, the measurements with the beam focused near the sample in the sample cavity were performed at the same P-T conditions as the sample measurements.

III. RESULTS

Raman spectra measured from the basal plane (0001) (wave vector **q** is perpendicular to the sample plane) with the excitation energy E_i=2.41 eV (514 nm) are shown in Fig. 1. All spectra were corrected by dividing to the Bose factor $[1-\exp(-\hbar\omega/kT)]^{-1}$ to account for the temperature-dependent intensity factor. A structureless background with the superimposed E_{2g} phonon line near 165 cm^{-1} was observed in the low-pressure spectra taken at all temperatures, similar to previous measurements at ambient pressure.[21] Here we report an appearance of a well-defined ELS peak near 580 cm^{-1} at 10 K for pressures higher than 20 GPa with an intensity that is increased by more than one order of magnitude. A broad peak near 620 cm^{-1} was also observed in the spectra excited with the 488 nm wavelength. The spectra obtained from the $(10\bar{1}0)$ plane with the same incident energy are presented in Fig. 2. In this geometry, the structureless background is observed below 20 GPa at all temperatures. It transforms to a pronounced electronic peak at 350 cm^{-1} at T=10 K under further pressure increase. Figure 3 shows that peak intensities start to grow sharply at a pressure of about 25 GPa. When the temperature is increased the electronic spectra smear out and become structureless. For $\mathbf{q}\|[0001]$ orientation a decrease in intensity at high temperature by a factor of about 2.5 was also found while the intensity for $\mathbf{q}\|[10\bar{1}0]$ was even higher at T=300 K in comparison to that at T=10 K.

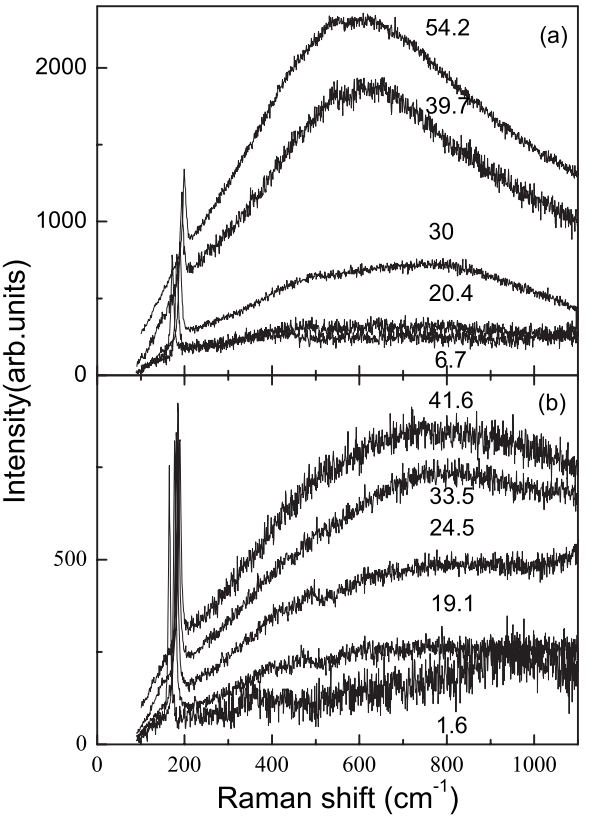

FIG. 1. Raman spectra at different pressures (GPa) measured from the (0001) plane at (a) T=10 and (b) 300 K, E_i=2.41 eV.

At the same time, the spectra measured with red and infrared excitation energies which probe smaller wave-vector values (Fig. 4) show only moderate evolution. The well-defined zero-pressure electronic peaks soften under pressure by ~10% without apparent changes in the linewidth. The

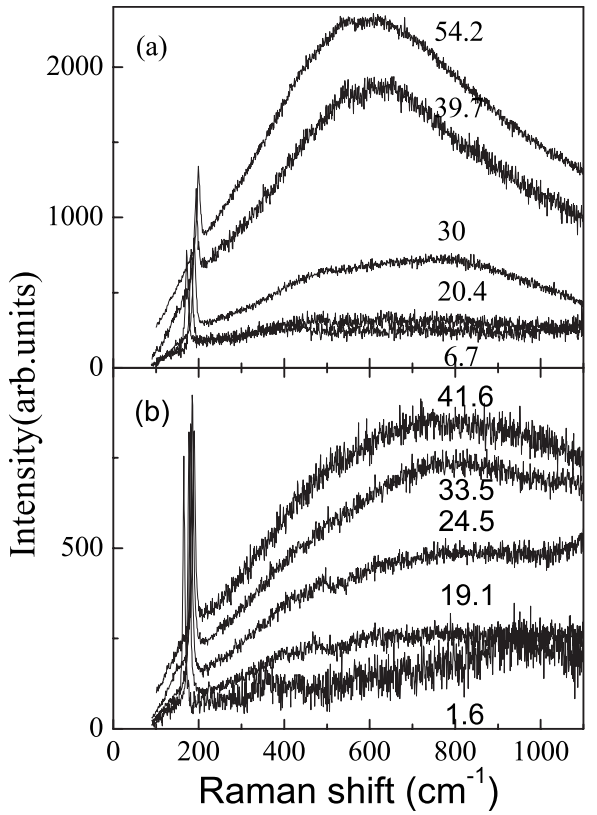

FIG. 2. Raman spectra at different pressures (GPa) measured from $(10\bar{1}0)$ plane at (a) $T=10$ and (b) 300 K, $E_i=2.41$ eV.

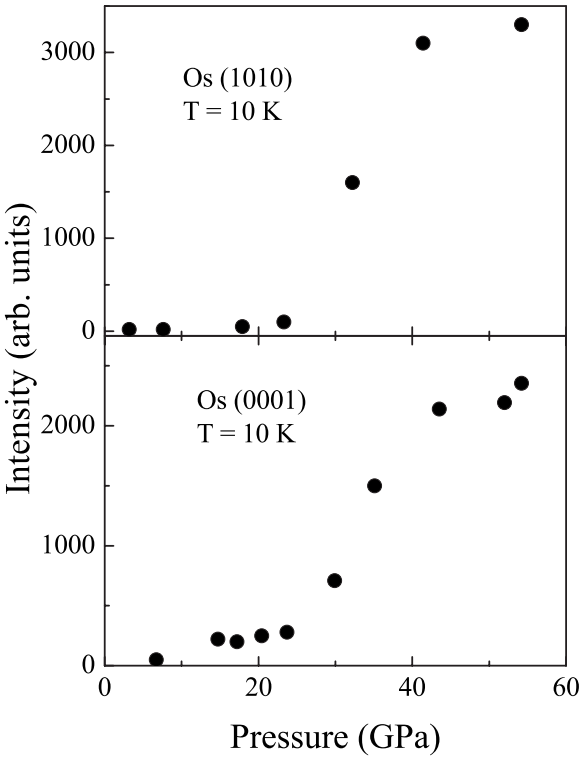

FIG. 3. The ELS peak intensity vs pressure for both **q** directions (after subtraction of low-pressure structureless background intensity), $T=10$ K, and $E_i=2.41$ eV.

spectra also show much lower **q** anisotropy (~10%) and their intensity increases by not more than a factor of 2. The maxima of the electronic peaks measured with $E_i=1.96$ eV (633 nm) excitation are located at 180 cm^{-1} ($\mathbf{q}\|[10\bar{1}0]$) and 200 cm^{-1} ($\mathbf{q}\|[0001]$) (Fig. 5). Their positions decrease further in frequency when using the near infrared excitation lines at $E_i=1.68$ eV (740 nm). For the $\mathbf{q}\|[0001]$ orientation the continuum is observed near 135 cm^{-1} at the highest pressure in our measurements (Fig. 5). The decrease in the wave-vector anisotropy with a decrease in the excitation energy was found in the previous measurements at ambient pressure,[21] where at $E_i=1.83$ eV (676 nm) the electronic peak position for $\mathbf{q}\|[0001]$ became even smaller than the corresponding peak position for $\mathbf{q}\|[10\bar{1}0]$ (Fig. 6).

The anomalies of the optical phonon self-energies were also found in the pressure range of 20–30 GPa. These effects will be reported elsewhere. Besides the one-phonon scattering a two-peak feature at 200–500 cm^{-1} is seen in the spectra shown in Figs. 1 and 2, which is assigned to the second-order phonon Raman scattering. For the $\mathbf{q}\|[10\bar{1}0]$ its intensity increases in the pressure range of 20–30 GPa at 300 K by an order of magnitude similar to the sharp increase in the electronic scattering intensity. At low temperatures the intensity of the two-phonon scattering is much weaker, so it remains unclear whether this effect holds.

The presented results reveal an abnormal pressure behavior of the light-scattering spectra by electrons and phonons above 20 GPa. First, an anomalous intensity increase in the ELS occurs with blue and green excitation energies accompanied by the transformation of the structureless background into well-defined electronic continuum peaks between 20 and 30 GPa. Second, the intensity of the two-phonon Raman scattering for $\mathbf{q}\|[10\bar{1}0]$ demonstrates a similar anomalous increase. Third, we observe different temperature dependences of the ELS intensity under pressure for both investigated wave-vector directions. Also, similar to what already reported at ambient pressure,[21] we observe a large downward shift in the electronic peak positions under pressure accompanied by a decrease in those peak anisotropies as the excitation energy is decreased.

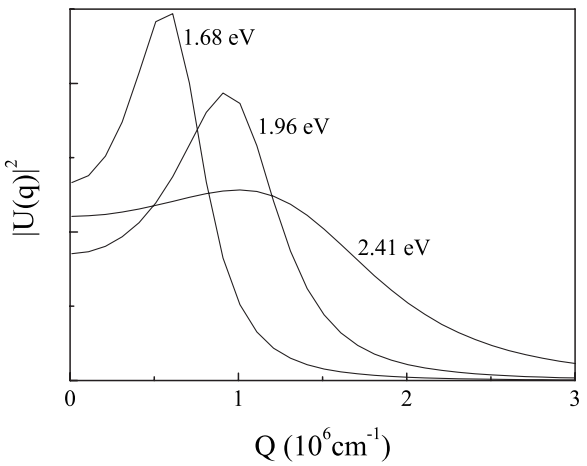

FIG. 4. The wave-vector distributions $|U(q)|^2$ for different incident energies. The expression is given in Sec. IV.

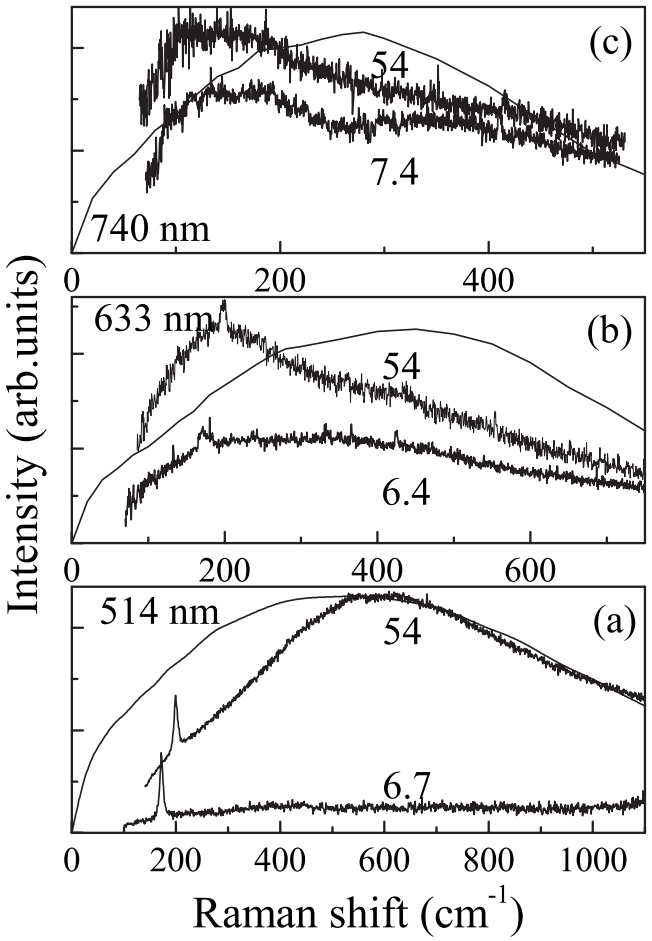

FIG. 5. The measured for $\mathbf{q}\|[0001]$ high and low-pressure Raman spectra and the calculated ELS spectra (50 GPa) for different excitation energies, $T=10$ K. (a) $E_i=2.41$ eV (514 nm), (b) $E_i=1.96$ eV (633 nm), and (c) $E_i=1.68$ eV (740 nm).

IV. CALCULATIONS

In order to understand the reasons for the observed anomalies we performed the calculations of the frequency-dependent ELS in the approximation of noninteracting electron-hole pairs. To determine the intensity of the intraband ELS we integrated the imaginary part of the polarization operator over the whole FS, taking into account the distribution of the incident and scattered fields in a metal,[19,20]

$$I(\omega,\mathbf{q}) \propto -\Im \int_{-\infty}^{+\infty} \frac{dq}{2\pi} |U(q)|^2 \int \frac{dS_p}{v} |\bar{\gamma}(p,q,\omega)|^2 \times \frac{q v_q}{\omega - q v_q + i\Gamma}, \tag{1}$$

where v_q is a projection of the Fermi velocity to the $\mathbf{q}$ direction and $\bar{\gamma}_{\alpha\beta}(p,q,\omega)=\gamma_{\alpha\beta}(p)-\langle\gamma_{\alpha\beta}(p)\rangle$, where the angle brackets denote the FS averaging,

$$\langle\gamma_{\alpha\beta}(p)\rangle = \int \frac{dS_p}{v}\gamma(p) \times \frac{q v_q}{\omega - q v_q + i\Gamma} \times \left(\int \frac{dS_p}{v} \frac{q v_q}{\omega - q v_q + i\Gamma} \right)^{-1}. \tag{2}$$

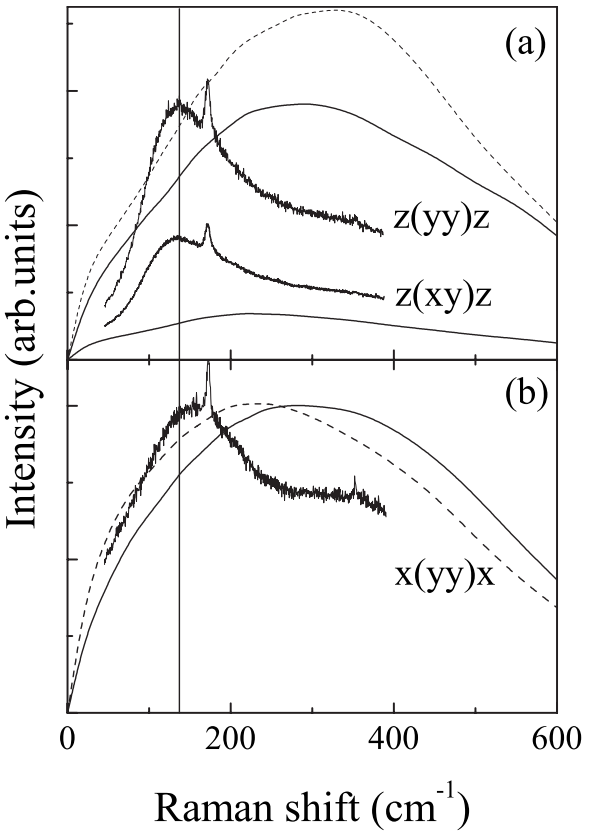

FIG. 6. The measured (taken from Ref. 21) and calculated (solid lines are nonresonant case and dashed lines are resonant) ELS spectra for both $\mathbf{q}$ directions and different polarization geometries. $E_i=1.83$ eV, $P=0$ GPa, and $T=10$ K. The vertical line marks the position of the ELS spectra with $\mathbf{q}\|[0001]$.

The integration over the wave-vector distribution $|U(q)|^2$ allows us to make the comparison to the ELS spectra for different excitation energies and to take into account the smearing of the spectra due to the absorption of the electromagnetic wave in the skin layer. The $|U(q)|^2$ function (shown in Fig. 4) can be expressed as $|U(q)|^2=4|\xi|^2/|q^2-\xi^2|^2$,[19,20,34] where $\xi=\xi_1-i\xi_2=(4\pi/\lambda_i)\cdot(n-ik)$, and n and k were measured for osmium in Ref. 33. The impurity relaxation frequency Γ was taken to be equal to the small value of 10 cm^{-1} for our high-purity samples. The electron-photon matrix element for intraband scattering generally can be given as[1,34]

$$\gamma_{\alpha\beta}(p) = e_\alpha^{(i)} e_\beta^{(s)} + \frac{1}{m}\sum_b \frac{p_{ba}^\beta p_{ab}^\alpha}{\epsilon_a(p) - \epsilon_b(p) + \omega_i + i\nu_b} + \frac{p_{ba}^\beta p_{ab}^\alpha}{\epsilon_a(p) - \epsilon_b(p) - \omega_s - i\nu_b}, \tag{3}$$

where $e_\alpha^{(i)}, e_\beta^{(s)}$ are the polarization vector components for the incident and scattered lights, p_{ba}^β is the electron momentum matrix element, m and $\epsilon_a(p)$ are the electron mass and energy, and the dependence on $\mathbf{q}$ is neglected here for the interband transition. The subscript a denotes the index of the band which crosses E_F and ν_b is the damping of the band b.

Its second term provides the resonance electronic scattering if the energy of incoming (scattering) light $w_{i,s}$ is equal to the energy difference $[\epsilon_a(p)-\epsilon_b(p)]$ between the Fermi energy and the bands $\epsilon_b(p)$ far from it. When the excitation energies are smaller than any interband transition energy, this matrix element reduces to the reciprocal effective-mass tensor (FS curvature)[35]

$$\gamma_{\alpha\beta}(p) = m\frac{\partial^2 \epsilon(p)}{\partial p_\alpha \partial p_\beta}. \quad (4)$$

The experimental data give an evidence of ELS resonance near $E_i \approx 2.2-2.3$ eV at ambient pressure and for its enhancement under the application of pressure.[21] On the other hand, the measurements with infrared excitations may represent a nonresonant case. At ambient pressure nearly equal ELS spectra intensities were observed for all three crystallographic wave-vector **q** directions [0001], [11$\bar{2}$0], and [10$\bar{1}$0] which probe rather different sections of the FS.[21] This suggests a resonance enhancement for the whole FS. Moreover, the observed resonance has a rather large width of ~0.5 eV and does not distort the continua line shapes. Thus, we used a constant $\bar{\gamma}(p,q,\omega)$ to simulate the resonant conditions (which suggests that the interband matrix elements of the momentum operator and energy denominators are constant in the **p** space) in addition to performing calculations with a nonresonant matrix element [Eq. (4)].

The band-structure calculations were performed using linearized muffin-tin orbital (LMTO) method[36] in the local-density approximation (LDA).[37] In the course of self-consistency a mesh of 1728 *k* points in the irreducible part of the Brillouin zone was used. Integration over the Fermi surface was performed with a fine mesh of 125 000 *k* points in the full Brillouin zone. The calculations of the first and second derivatives of the electron energies were performed using the OPENDX package. The band-structure calculations were performed with and without including the spin-orbit interaction for the Os 5*d* states. The spin-orbit coupling was directly introduced in the code as opposed to the often-used second variation procedure. Specifically we worked with doubled (due to the spin) full-orbital Hamiltonian taking into account the spin-orbit interaction explicitly, and the variational procedure was performed in one step.

The obtained FS, shown in the inset of Fig. 7 (see also a very clear Fig. 3 in Ref. 41), is in agreement with that calculated previously.[38–41] It consists of four main sheets: electronic ones $\Gamma 9e$ (sheet names from Ref. 38) and $\Gamma 10e$, small hole sheets *U*7*h* in the *LM* direction, and a complicated anisotropic "monster" surface *KM*8*h*. Our calculations were performed for the lattice parameters and volumes corresponding to 0 and 50 GPa.[29] As in Refs. 40 and 41 in this pressure region no changes in the FS topology were found. The main effect of neglecting the spin-orbit interaction is the preservation of the degeneracy of the ninth and tenth bands in the ΓA direction. This results in a small change in the $\Gamma 9e$ and $\Gamma 10e$ sheet geometries near this direction, giving a negligible effect in the calculated spectra. However, it was noted earlier[36] that the inclusion of the spin-orbit interaction in Os is crucial for the existence of small FS sheets near the *L* and

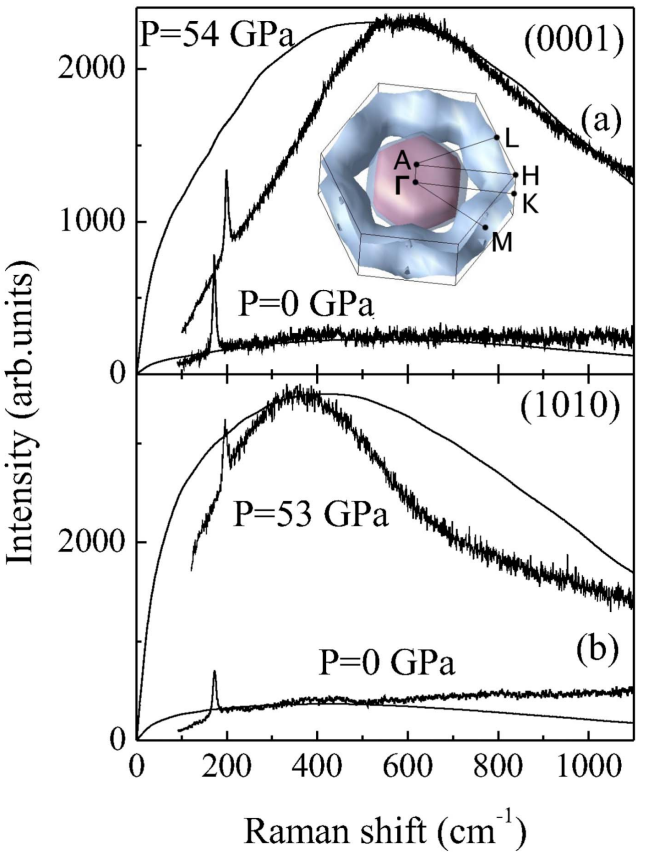

FIG. 7. (Color online) The measured and calculated [from Eq. (1)] ELS high and ambient pressure spectra for (a) $\mathbf{q}\|[0001]$ and (b) $\mathbf{q}\|[10\bar{1}0]$. $T=10$ K and $E_i=2.41$ eV. The calculated intensities were normalized to the measured ones. The calculated FS is shown in the inset.

Γ points. In our case the most interesting effect, as we will see below, consists of possible changes to the FS topology near the *L* point due to its dynamical modification caused by the E_g phonons.

Figure 7 shows a rather close correspondence of the measured and calculated high-pressure ELS spectra for both **q** directions with the $E_i=2.41$ eV excitation (resonant case). In particular, both measured and calculated spectra show almost linear behavior at low frequencies. This suggests that the observed ELS spectra are related to the intraband transitions. On the other hand, experimental ELS spectra show narrower peaks than predicted from calculations, and they are sometimes shifted with respect to the calculated ones (especially for red and near infrared excitations) (Figs. 5–7). Because of the topology of the calculated $\Gamma 9e$ and $\Gamma 10e$ sheets, which look like hexagonal prisms and have large areas at the side and top (bottom) surfaces, these areas provide enhanced contributions to the scattering cross section at low frequencies because of the small electron velocity projections along the crystal axis and in-plane wave-vector directions, respectively. The same is true for the *KM*8*h* sheet which contributes ~40% of the spectral weight in the calculated intensity for resonant conditions. It is plausible that the difference in experimental and theoretical ELS spectra may be due to a

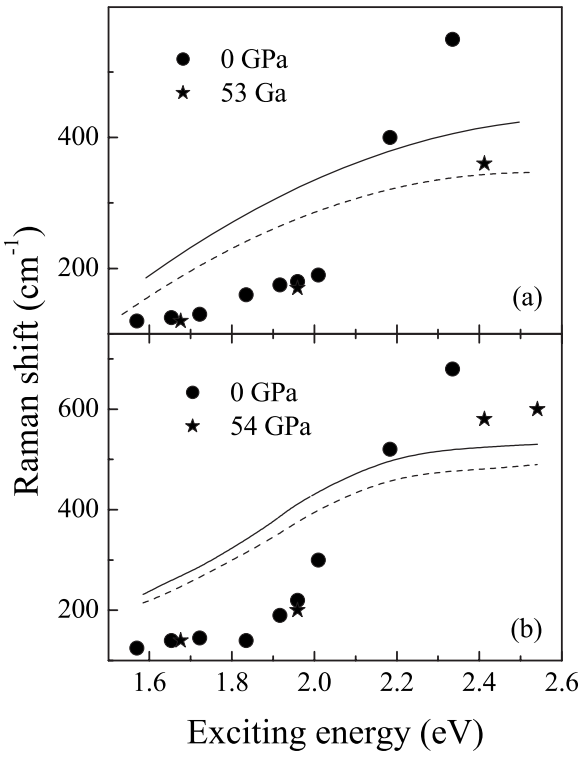

FIG. 8. The measured (points) and calculated (dashed lines at 0 GPa and solid lines at 50 GPa) ELS maxima positions vs E_i for (a) $\mathbf{q}\|[10\bar{1}0]$ and (b) $\mathbf{q}\|[0001]$, where $T=10$ K.

more complex FS topology and/or the velocity distribution at the FS with the interactions included.

A comparison of the calculated and measured continua frequencies for the different excitation energies and pressures in Fig. 8 also supports this hypothesis. At the excitation energies $E_i<2.2$ eV the calculated frequencies substantially exceed (up to two times) the measured ones. For the excitation energies of $E_i>2.2$ eV the calculations predict at all pressures well-defined electronic peaks at frequencies that are smaller than those corresponding to the observed structureless electronic continua (Figs. 1, 2, and 7). The appearance of pronounced peaks in the spectra measured at pressures $P\geq 20$ GPa improves the agreement with the calculation in this excitation energy range. The calculated spectra become harder and broader under pressure by ~10% for $\mathbf{q}\|[0001]$ and ~20% for $\mathbf{q}\|[10\bar{1}0]$ at all excitation energies, and their intensities decrease at the same ratio. This contradicts the observed strong intensity growth, the electronic peak position softening, and narrowing when using excitations in the blue-green range compared to only a negligible frequency softening with the red excitation.

The $\mathbf{q}$ anisotropy of the electronic peak frequencies calculated with a constant $\bar{\gamma}(p,q,\omega)$ does not depend on E_i, which is in contrast to the observed decrease with the red and near infrared excitations. The ELS spectra calculated for the nonresonant case [matrix element from Eq. (4)] show (Fig. 4) a decrease in the anisotropy of the frequencies measured with the red excitation for the studied $\mathbf{q}$ directions. This is in close agreement with the experimental measurements. However, the intensities and frequencies of the calculated depolarized spectra in the $Z(XY)Z$ geometry (E_{2g} symmetry) for the red and near infrared excitations were found to be lower than those observed in experiment at ambient pressure (Fig. 6). It should also be noted that screening does not change the intensities and the peak line shapes substantially for the (XX) and (YY) polarization geometries obtained for all four FS sheets, indicating that the screened component of A_{1g} symmetry $\bar{\gamma}_{\alpha\beta}(p,q,\omega)$ is approximately equal to the bare $\gamma_{\alpha\beta}(p)$. Intrasheet screening is almost absent for the $KM8h$ sheet $[\langle\gamma_{\alpha\beta}(p)\rangle\approx 0]$ but has a large magnitude of ~90% for the $U7h$ sheet. This indicates a significant contribution of intersheet mass fluctuations to the calculated screened intensity in the parallel polarization geometry which is mostly due to small $U7h$ ellipsoids. The contribution of this intersheet scattering as well as the contribution of the bare (XX) and (YY) components (E_{2g} symmetry) from the $U7h$ sheet is comparable with the intrasheet scattering from the $KM8h$ sheet. A large FS curvature of the $U7h$ sheet provides a large electronic scattering cross section (especially at the resonance conditions), showing that even small sheets may contribute significantly into the net scattering efficiency.

All presented calculations correspond to static case, i.e., they do not include the phonon displacements which, in principle, can modify the fine electronic structure near E_F and the Fermi-surface topology in dynamics. As was shown earlier,[21] E_{2g} phonons in Os interact strongly with the low-frequency electronic excitations, resulting in changes to their energy and linewidth. A more detailed understanding of the coupling of this phonon with the electronic structure is obtained by calculating the Os band structure with atom displacements corresponding to the E_{2g} degenerate phonon mode. The atoms in two layers of hcp lattice are displaced out of phase in X or Y directions in this mode. In Figs. 9 and 10 we present the Os band structure for $+u$ and $-u$ displacements in the X direction for two pressures: 0 and 50 GPa. The energy of this mode, by symmetry, is an odd function of displacement, and we found strong changes in the Fermi-surface topology under pressure in comparison to a much smaller modification for the second E_{2g} mode with displacements along the Y direction. Displacements of ~0.04 Å were used which are close to the root-mean-square displacements for zero-point motion in osmium. As shown in Figs. 9 and 10, under a $+u$ displacement, the bands near the L point cross the Fermi level under pressure while under a $-u$ displacement the band energy goes down. At the same time the bands near the Γ point which were found to determine the topological transition under pressure[41] do not show such radical changes. Thus, this result suggests that the dynamic electronic topological transition (ETT) is possible in Os under pressure (cf. static ETT at higher P proposed in Ref. 41).

V. DISCUSSION

The discrepancy between the experimental and calculated spectra (Figs. 5–8) suggests that electron-scattering mechanisms not included in the LDA approximation are important for this system. A substantial increase in the calculated ELS peak frequencies in comparison to the measured ones (Fig. 8) occurs in the range of 200–500 cm^{-1}, i.e., in the energy

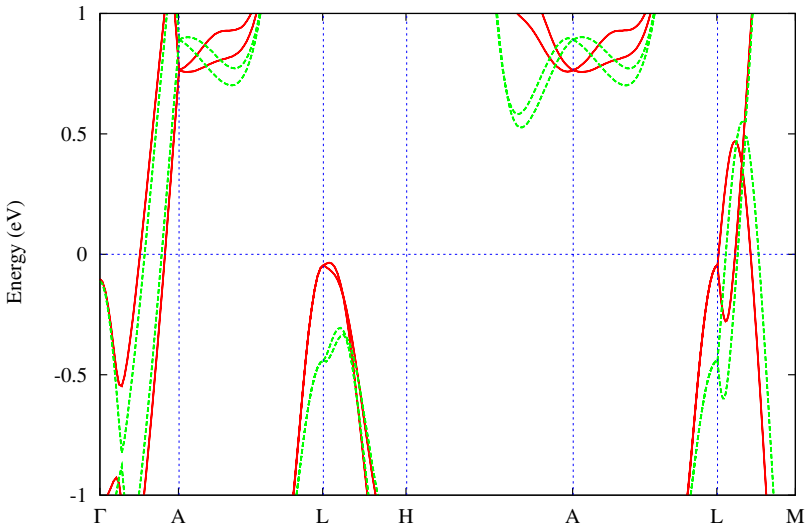

FIG. 9. (Color online) Band structure obtained within the LDA approach *with* spin-orbit coupling with $+u$ (red, solid) and $-u$ (green, dashed) distortions in the X direction. Fermi level corresponds to zero energy.

region of the phononic excitations of osmium. Strong temperature effects at all pressures also suggest an important role of the inelastic e-ph scattering.[14–17] Thus, the e-ph interaction may be the reason of discrepancy found in the low-energy range, leading to the electron dispersion renormalization at small $\mathbf{q}$ (low-energy excitation, see Fig. 4).

The observation of the structureless electronic background at low pressures with $E_i > 2.2$ eV provides evidence for the increase in the damping of the electronic states for large wave vectors $\mathbf{q}$, an essential part of which is probed by the high-energy excitation (Fig. 4). This implies the existence of additional scattering mechanisms for electronic states lying away from the Fermi energy by $500-1000$ cm^{-1}. The Fermi-surface topology [inset of Fig. 5(a)] having large nearly parallel sections of the FS with wave vectors Q in the basal plane favors an enhancement of the e-e scattering.

An anomalous growth of the two-phonon cross section under pressure for $\mathbf{q} \| [10\bar{1}0]$ at $T = 300$ K supports this suggestion. It was shown theoretically[42] that such an enhancement of the two-phonon Raman spectra in transition metals may be due to successive phonon ω_{+Q} and ω_{-Q} emissions between electronic states close to the Fermi level when the conditions for double-photon resonance are fulfilled. If the condition $\omega_{+Q} + \omega_{-Q} \approx v_F \times \mathbf{q}$ is fulfilled, the same resonance mechanism may provide an anomalous ELS intensity growth under pressure due to an extended region of phase space for the scattering events. This is possible if the leading resonance term is determined by the scattering processes near the Fermi level having energy denominators with a small damping. The correlation of the peak narrowing with the ELS intensity increase under pressure supports this possibility. Both final states consisting of one phonon plus an electron-hole pair and two-pair final state will provide an electronic background which could interfere with the two-phonon Raman scattering.[42] In turn, the decrease in the electronic damping at high-energy excitation (probing larger $\mathbf{q}$ magnitudes) may be due to both the electron and phonon spectra

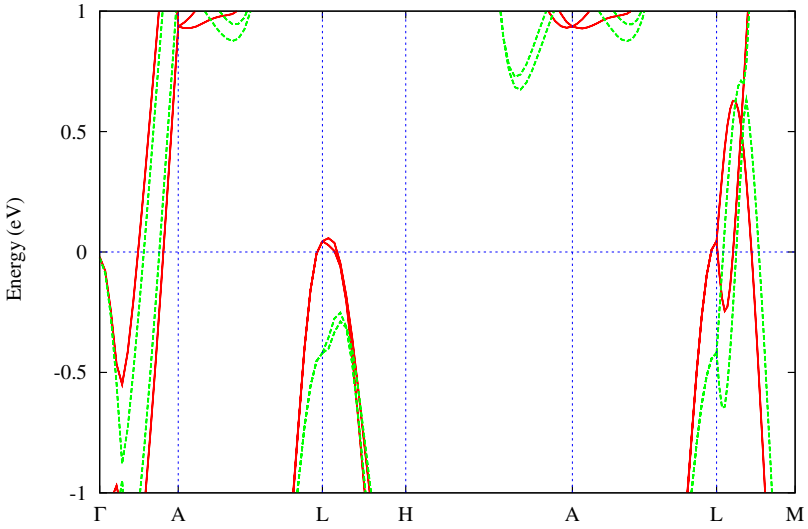

FIG. 10. (Color online) Band structure obtained within the LDA approach with spin-orbit coupling for $P = 50$ GPa with $+u$ (red, solid) and $-u$ (green, dashed) distortions in the X direction. Fermi level corresponds to zero energy.

change and the interplay of the e-ph and e-e scattering contributions which determine the **q** and ω dependence of the effective e-ph coupling.[43]

Another possible scenario for the anomalous ELS cross section increase under pressure is the appearance of a new Fermi-surface sheet. However, none of the previous calculations of osmium band structure at high pressure[40,41] shows the FS topology change in the investigated pressure range. First ETT was found at 72 GPa (ellipsoid appearance at the Γ point) and two more occur near the L point at pressures of 81 and 122 GPa.[41] All new features are rather small (density of states is less than that of the $U7h$ sheet) and may give a strong contribution only owing to a strong resonance. Our calculations show (Fig. 9) that the displacements of two atoms in the Os cell modeling one of the degenerate E_{2g} modes (with atoms moving along X direction) lead to a strong band shift near the L point and a dynamical FS topology change under pressure. Thus, the phonon-assisted Lifshitz transition[44] may occur at pressures lower than those calculated in Ref. 41. This may also be a reason for the c/a anomaly found in Ref. 29, although this result was not confirmed in an independent study.[45] The E_{2g} phonon anomalies found at ambient and high pressures may also be coupled with the strong band structure changes near the L point. The band-structure calculations performed in this work and in Ref. 41 also showed that the interband transitions near the L point with magnitude of $\sim$2.5 eV may provide the resonance conditions, and hence, the possibility of observing the ELS coupled with this feature. The unusual temperature behavior of the ELS intensity for the studied **q** directions remains unclear. It is natural to expect similar temperature behavior if the observed electronic scattering is determined by large FS sheets. Another possibility may arise if this scattering originates from the electronic states near the L point which are strongly coupled to the phonons, and anisotropic electronic structure changes under the varying pressure and temperature conditions.

The comparison of the ELS spectra calculations performed for the resonant and nonresonant cases (Fig. 6) suggests that a decrease in the electronic peak position anisotropy (for the studied **q** directions) at smaller excitation energies may be explained by a change in the p dependence of the electron-photon matrix element. In this simple calculation, a constant matrix element was used for the resonant case. This implies that the whole FS is in resonance which is possible for a small FS sheet but is not realistic for the main osmium FS sheets. Detailed band-structure calculations of the resonant behavior are necessary for better understanding of the ELS cross section increase with the high-energy excitation. These calculations are also needed to explain why the ratio of polarized and depolarized spectra intensities and frequencies for $\mathbf{q}\|[0001]$ is conserved while the frequency anisotropy for the studied **q** varies strongly upon the excitation energy change.

VI. CONCLUSIONS

Raman studies of osmium under pressure showed an anomalous increase in the ELS cross section measured with the blue and green incident energies. In the pressure range of 20–30 GPa the low-temperature structureless background transformed to pronounced peaks at $\sim$580 cm^{-1} for $\mathbf{q}\|[0001]$ and at $\sim$350 cm^{-1} for $\mathbf{q}\|[10\bar{1}0]$ showing strong temperature dependencies. The discrepancy between frequency behavior and line shapes of the measured Raman spectra and those calculated within the LDA provides evidence for the electron self-energy renormalization in the energy range $\sim$1000 cm^{-1} from the Fermi level due to e-ph and e-e scatterings. Changes in the FS topology were found in the band-structure calculation including the E_{2g} phonon displacements. We suggest that this effect may constitute the primary contribution to the ELS spectra observed in resonant conditions. Clear understanding of these anomalies requires the detailed calculations of the resonance effects and taking into account the phonon renormalization on the electron band structure. Further studies of the ELS spectra under pressure and temperature variations are necessary to further understand the details of the e-ph coupling.

ACKNOWLEDGMENTS

We thank E. G. Maksimov, I. I. Mazin, R. J. Hemley, and H.-K. Mao for helpful discussions. This research was supported by RFBR under Grant No. 08-02-00437, Carnegie Institution of Washington, DOE/BES, DOE/NNSA (CDAC), NSF, and the W. M. Keck Foundation. S.V.S. appreciates the support from the Dynasty Foundation, Russian Ministry of Science and Education, CRDF Foundation (Grant No. Y4-P-05-15), Ural division of RAS and acknowledges the support of President of Russia Grant for YS (Grant No. MK-1184.2007.2).

*ponosov@imp.uran.ru

[1] S. B. Dierker, M. V. Klein, G. W. Webb, and Z. Fisk, Phys. Rev. Lett. **50**, 853 (1983).
[2] R. Sooryakumar and M. V. Klein, Phys. Rev. Lett. **45**, 660 (1980).
[3] M. V. Klein and S. B. Dierker, Phys. Rev. B **29**, 4976 (1984).
[4] R. Hackl, R. Kaiser, and S. Schicktanz, J. Phys. C **16**, 1979 (1983).
[5] S. L. Cooper, M. V. Klein, B. G. Pazol, J. P. Rice, and D. M. Ginsberg, Phys. Rev. B **37**, 5920 (1988).
[6] T. Staufer, R. Hackl, and P. Muller, Solid State Commun. **75**, 975 (1990).
[7] A. A. Maksimov, I. I. Tartakovskii, V. B. Timofeev, and L. A. Falkovskii, Sov. Phys. JETP **70**, 588 (1990).
[8] M. C. Krantz, H. J. Rosen, J. Y. T. Wei, and D. E. Morris, Phys. Rev. B **40**, 2635 (1989).
[9] P. Nyhus, S. L. Cooper, and Z. Fisk, Phys. Rev. B **51**, 15626 (1995).

[10] P. Nyhus, S. L. Cooper, Z. Fisk, and J. Sarrao, Phys. Rev. B **52**, 14308(R) (1995); **55**, 12488 (1997).
[11] C. M. Varma, P. B. Littlewood, S. Schmitt-Rink, E. Abrahams, and A. E. Ruckenstein, Phys. Rev. Lett. **63**, 1996 (1989).
[12] A. Zawadowski and M. Cardona, Phys. Rev. B **42**, 10732 (1990).
[13] A. Virosztek and J. Ruvalds, Phys. Rev. B **45**, 347 (1992).
[14] S. V. Shulga, O. V. Dolgov, and E. G. Maksimov, Physica C **178**, 266 (1991).
[15] V. N. Kostur and G. M. Eliashberg, JETP Lett. **53**, 391 (1991).
[16] S. N. Rashkeev and G. Wendin, Z. Phys. B: Condens. Matter **93**, 33 (1993).
[17] K. Itai, Phys. Rev. B **45**, 707 (1992).
[18] B. S. Shastry and B. I. Shraiman, Phys. Rev. Lett. **65**, 1068 (1990); J. K. Freericks, T. P. Devereaux, and R. Bulla, Phys. Rev. B **64**, 233114 (2001).
[19] I. P. Ipatova, M. I. Kaganov, and A. V. Subashiev, Sov. Phys. JETP **57**, 1006 (1983).
[20] L. A. Falkovsky, Zh. Eksp. Teor. Fiz. **103**, 666 (1993) [JETP **76**, 331 (1993)].
[21] Yu. S. Ponosov, G. A. Bolotin, C. Thomsen, and M. Cardona, Phys. Status Solidi B **208**, 257 (1998).
[22] I. P. Ipatova and A. V. Subashiev, Sov. Phys. JETP **39**, 349 (1974).
[23] E. G. Maksimov and S. V. Shulga, Solid State Commun. **97**, 553 (1996).
[24] Yu. S. Ponosov, I. Loa, V. E. Mogilenskikh, G. A. Bolotin, and K. Syassen, Phys. Status Solidi C **1**, 3114 (2004).
[25] Yu. S. Ponosov, I. Loa, V. E. Mogilenskikh, and K. Syassen, Phys. Rev. B **71**, 220301(R) (2005).
[26] Yu. S. Ponosov, Sov. Phys. Solid State **23**, 861 (1981).
[27] Yu. S. Ponosov, G. A. Bolotin, G. P. Kovtun, and V. E. Elenskii, Sov. Phys. Solid State **26**, 491 (1984).
[28] Yu. S. Ponosov and G. A. Bolotin, Phys. Status Solidi B **215**, 137 (1999).
[29] F. Occelli, D. L. Farber, J. Badro, C. M. Aracne, D. M. Teter, M. Hanfland, B. Canny, and B. Couzinet, Phys. Rev. Lett. **93**, 095502 (2004).
[30] G. J. Piermarini, S. Block, J. D. Barnett, and R. A. Forman, J. Appl. Phys. **46**, 2774 (1975).
[31] S. Buchsbaum, R. L. Mills, and D. Schiferl, J. Phys. Chem. **88**, 2522 (1984).
[32] S. Merkel, A. F. Goncharov, H. K. Mao, P. Gillet, and R. J. Hemley, Science **288**, 1626 (2000).
[33] V. V. Nemoshkalenko, V. N. Antonov, V. N. Antonov, M. M. Kirillova, A. E. Krasovskie, and L. V. Nomerovannaya, Sov. Phys. JETP **63**, 115 (1986).
[34] L. A. Falkovsky and S. Klama, Phys. Rev. B **50**, 5666 (1994).
[35] A. A. Abrikosov and L. A. Falkovskii, Sov. Phys. JETP **13**, 179 (1961).
[36] O. K. Andersen and O. Jepsen, Phys. Rev. Lett. **53**, 2571 (1984).
[37] We used alternatively the general gradient approximation (GGA), as it was proposed by Perdew-Wang (PW91). However, no significant changes of the band structure were found near the Fermi level.
[38] O. Jepsen, O. K. Andersen, and A. R. Mackintosh, Phys. Rev. B **12**, 3084 (1975).
[39] V. I. Smelyansky, A. Y. Perlov, and V. N. Antonov, J. Phys.: Condens. Matter **2**, 9373 (1990).
[40] Y. Ma, T. Cui, L. Zhang, Y. Xie, G. Zou, J. S. Tse, X. Gao, and D. D. Klug, Phys. Rev. B **72**, 174103 (2005).
[41] D. Koudela, M. Richter, A. Mobius, K. Koepernik, and H. Eschrig, Phys. Rev. B **74**, 214103 (2006).
[42] M. V. Klein, Phys. Rev. B **24**, 4208 (1981).
[43] R. Zeyher and M. L. Kulic, Phys. Rev. B **53**, 2850 (1996).
[44] A. F. Goncharov and V. V. Struzhkin, Physica C **385**, 117 (2003).
[45] T. Kenichi, Phys. Rev. B **70**, 012101 (2004).